In: 1st Workshop on Low-Cost Digital Solutions for Industrial Automation, 25-26 September 2023, Cambridge, UK
https://doi.org/10.1049/icp.2023.1748

Low-Cost Vibration Sensor with Low Frequency Resonance for Condition Monitoring of Low Speed Bearings: A feasibility study

Agusmian Partogi Ompusunggu[1] and Cristobal Ruiz Carcel[1]

[1] *Centre for Life-Cycle Engineering and Management (CLEM), SATM, Cranfield University, College Road, MK43 0AL, UK*
**Email: agusmian.ompusunggu@cranfield.ac.uk*

Abstract

Condition monitoring (CM) of rolling element bearings (REBs) rotating at low speeds poses some challenges in practice because of the low signal-to-noise ratio produced by the faults. Both vibration-based and ultrasound/acoustic emission (AE) based sensing techniques have been proposed in the literature to detect faults in rolling element bearings running at low speeds. The vibration-based technique generally works within the frequency band from 0 to 20 kHz. Meanwhile, the ultrasound/AE-based techniques work in a very high-frequency band, from 20 kHz up to 1 MHz. Consequently, processing ultrasound/AE sensor data requires more computational resources compared to processing vibration data. Moreover, the hardware investment to build an ultrasound/AE-based CM system is more expensive than that of a vibration-based CM system. Since hardware and software cost is one of the main bottlenecks of the adoption of CM systems in the industry, it is, therefore, necessary to develop a cost-effective vibration-based CM system for critical bearings mounted on low-rotational speed machines. The paper presents a feasibility study in evaluating the performance of an off-the-shelf low-cost vibration sensor (10 – 20 times cheaper than high-end vibration sensors) with a low resonance frequency (around 75 Hz) to diagnose faults on REBs operating at a low rotational speed of 30 - 60 rpm. The low-resonance frequency characteristic of the low-cost sensor allows us to acquire the data at a low sampling rate of 400 Hz. A theoretical justification of why a vibration sensor with low-resonance frequency can still be effective for low-speed bearing fault diagnosis is given. This feasibility was experimentally validated on a test rig on which an REB with a seeded fault on the outer race was tested as a case study. A high-end vibration sensor (accelerometer) acquired at a 20 kHz sampling rate was also used as a benchmark. The vibration signals measured by the low-cost and high-end sensors in four different operating conditions were analysed with the well-established envelope analysis. In addition, the high-end sensor signals were also analysed with the state-of-the-art Spectral Correlation (SC) technique to compute the Enhanced Envelope Spectrum (EES) for bearing fault detection and diagnosis. The results confirmed that the bearing fault could be successfully detected and diagnosed in all the test conditions by the low-cost sensor analysed with the envelope analysis technique. On the other hand, the high-end sensor analysed with the SC technique could only diagnose the bearing fault for the least challenging test condition. The outstanding diagnostic capability of the low-cost sensor sampled at a low sampling rate has set a milestone that would enable the future development of a low-cost CM system for low-speed bearing applications.

1 Introduction

The development of condition monitoring (CM) systems for rolling element bearings, hereafter called bearings, has been the main point of attentions in the predictive maintenance (PdM) research community for many decades because these mechanical components play a very vital role in the operation and availability of rotating machinery [1]. Despite successful implementations in real-life applications, CM of bearings still poses some challenges. One of the challenges is fault detection and diagnosis of bearings subject to low (rotational) speed. As signals generated by the faults of low-speed bearings are very weak and often covered by strong noise from other mechanical components such as gears, screws, etc., extracting the fault signatures from such signals is not an easy task [2–6]. Having a robust and reliable CM system for low-speed bearings will have significant impacts to reduce machines downtime in some industrial applications, including steel casting, paper mill, food industry, wind energy, etc, which leads to the operation and maintenance cost (OPEX) reduction.

Numerous methods have been developed for more than a decade for CM of low-speed bearings. In general, these methods can be divided into vibration-based [2, 4] and ultrasound/acoustic emission (AE) based methods [3, 6–8]. Despite the success of ultrasound/AE-based techniques for CM of low-speed bearings, high computational cost due to the requirement of high sampling rate as well as the hardware (preamplifiers and data acquisition) investment required for the sensors, are the most common drawbacks for these techniques. In the case of vibration-based techniques using conventional vibration sensors (i.e. frequency bandwidth up to 20 kHz), the fault diagnosis effectiveness for low-speed applications can be hindered due to the low signal-to-noise ratio [5].

Considering the advantage of the vibration-based techniques in terms of the sampling rate, as opposed to the counterpart ultrasound/AE-based techniques, one might raise a fundamental question of whether the vibration-based techniques can still be effective for fault diagnosis of low-speed bearings if the used sampling rate is much lower compared with the sampling rate used for common vibration sensors (accelerometers). If this question is addressed, hence, a more cost-effective CM solution for low-speed bearing applications can be realised.

This paper aims to address the raised question through a

feasibility study where a vibration sensor with low resonance frequency (in the range of tens Hz) is used for the first time for fault diagnosis of low-speed bearings. Using such a vibration sensor suggests that a sampling frequency of a few hundred Hz should be sufficient to acquire vibration signals. To justify this hypothesis and motive this feasibility study, a theoretical analysis of the effectiveness of a low resonance frequency vibration sensor for faults diagnosis of low-speed bearings is given in the following section.

The remainder of this paper is structured as followed. Section 2 presents the theoretical justification of why a vibration sensor with low-resonance frequency can still be used for fault diagnosis of low-speed bearing applications. Section 3 discusses the research methodology. Section 4 discusses the experimental procedure. Section 5 discusses the results obtained from the data analysis. Section 6 draws relevant conclusions and proposes future work.

2 Theoretical Justification

It is commonly accepted in the literature that a fault in operational bearings generates an impact force $F_i(t)$. As shown by Khanam et al., [9], the duration of the impact force is *inversely proportional* to the bearing rotational speed. This implies that the impact force duration of high speed bearings is shorter than that of low-speed bearings. Without loss of generality, let us assume that the impact force $F_i(t)$ is represented by a half sinusoidal signal:

$$F_i(t) = \begin{cases} F_0 \sin\left(\frac{\pi}{T_f} t\right), & 0 \leq t \leq T_f \\ 0 & \text{else,} \end{cases} \tag{1}$$

where F_0 denotes the impact force amplitude, t is the time, and T_f is the impact force duration. By applying the Fourier transformation to Eq. (1), one can analytically show that the frequency spectrum magnitude of the impact force signal can be expressed as follows, see Harris and Piersol [10]:

$$\begin{aligned} F(j\omega) &= \mathscr{F}\{F_i(t)\} \\ |F(j\omega)| &= J_0 \left| \frac{\cos(\omega T_f/2)}{1-(\omega/\omega_f)^2} \right| \end{aligned} \tag{2}$$

where $\mathscr{F}\{\cdot\}$ denotes the Fourier transformation operator, $|F(\omega)|$ denotes the frequency spectrum magnitude of the impact force signal $F_i(t)$, $J_0 = \frac{2F_0T_f}{\pi}$, $\omega_f = \frac{\pi}{T_f}$, $\omega = 2\pi f$, and f is the frequency in Hz. A careful examination on Eq. (2) shows that the frequency spectrum magnitude is *zero* at the frequency $f = \frac{3}{2T_f}$. These zero magnitudes are also observed at other frequencies, namely $\frac{5}{2T_f}$, $\frac{7}{2T_f}$, $\frac{9}{2T_f}$, etc.

Figure 1 illustrates the impact forces and the corresponding frequency spectra for different impact duration. It is seen that the frequency bandwidth of the impact force with a short duration is larger than the frequency bandwidth of the impact force with a longer duration. This suggests that the energy of the impact force generated by the faults in low-speed bearings is mainly concentrated at low frequency range. Therefore, for fault diagnosis of low-speed bearings, it is necessary to select a vibration sensor with the resonance frequency f_r within the main frequency bandwidth of the impact force i.e. $f_r < \frac{3}{2T_f}$. This way, the bearing fault signature in the vibration signals is amplified by the sensor resonance.

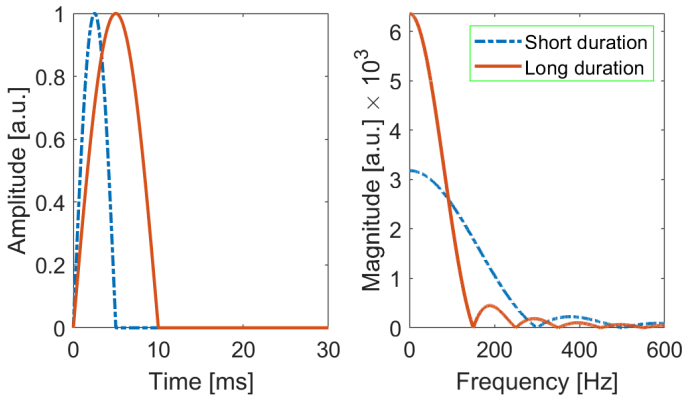

Figure 1: Simulated impact force $F_i(t)$ and the frequency spectrum $F(f)$ for different impact duration T_f.

3 Methodology

This section discusses three aspects, namely: (1) the selection of a low-cost off-the shelf sensor model with low resonance frequency from the market and a high-end accelerometer as a benchmark, (2) the design, manufacturing and assembly of a test rig dedicated for fault diagnosis of low-speed bearings, and (3) the signal processing method.

3.1 Sensor selection and data acquisition

A market scan was performed to select any low-cost off-the-shelf vibration sensor types with low resonance frequency (in the range of tens Hz). It was found that there was no so many options available on the market for a sensor with low resonance frequency, relatively small dimension and low cost. Through the market scan, a low-cost cantilever-type vibration sensor (the Minisense 100), which costs less than £10 per unit, was selected. The sensor weighs less than 1 gram, with a resonance frequency of around 75 Hz and a dimension of 1mm x 7mm x 18mm. Notably, this low-cost sensor needs to be coupled with a charge amplifier for the operation. For benchmarking, a high-end IEPE Dytran 3055D2 accelerometer, with 100 mV/g sensitivity and a frequency range of 1-10,000 Hz was selected.

3.2 Test rig design & assembly

The selected test bearing was an N 203 ECP bearing due to its size, minimum radial load and also the easiness of disassembly and reassembly, which facilitates seeding fault on the outer race. The 20 mm diameter shaft was supported by two angular contact bearings resulting in a cantilever configuration, with the test bearing located beyond the outermost bearing as shown in Figures 2 and 3. A structure of metal rods and bars was used to position the test-bearing housing axially and constrain rotation. Calibrated static radial loads were hung from the housing vertically. The shaft was driven by a Nema 23 stepper motor, model 23HS22-2804S-HG10, with a built-in 1:10 reduction gearbox. A dedicated controller was used to control the rotational speed.

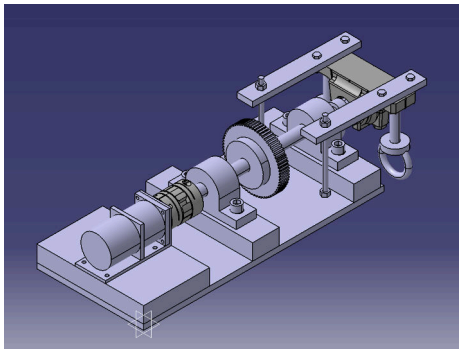

Figure 2: 3D CAD model of the test set-up.

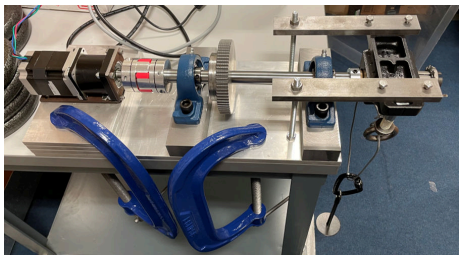

Figure 3: Final assembly of the test setup.

The high-end and low-cost sensors were mounted on a metal plate at the bottom of the bearing housing using high-strength adhesive to ensure an equivalent transmission path, see Figure 4. When installing the test bearing with an outer race defect, it is necessary to align the position of the defect to the bottom position of the bearing housing which corresponds to the load zone. This is done to ensure a realistic scenario where outer race defects are typically formed around the load zone. A couple of G-clamps were used to fix the base of the test setup on the experimental bench.

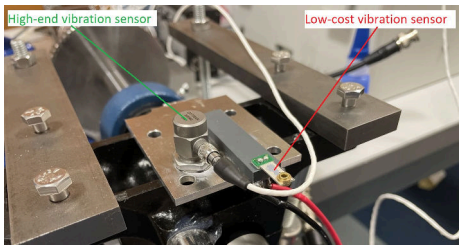

Figure 4: Sensors mounted on test setup.

3.3 Signal processing technique

For a fair comparison, the same signal processing technique for bearing fault diagnosis, based on the well-established envelope analysis method (see Randall [1]), was applied to the low-cost and high-end sensor signals. This method is graphically explained in Figure 5.

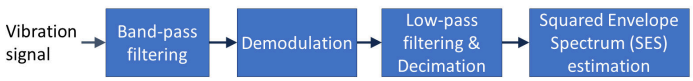

Figure 5: The block diagram of the envelope-based signal processing technique.

As the resonance frequency of the low-cost sensor is relatively low, prior to applying the envelope analysis, the low-cost sensor signals were decimated at a new sampling rate of 400 Hz. This way, the advantage of the low-cost sensor with a low sampling rate capability for low-speed bearing fault diagnosis can also be demonstrated.

The first step of the envelope analysis is band-pass filtering of the vibration signal around the resonance frequency of the low-cost sensor. The second step is demodulating the band-pass filtered signal to shift to a low-frequency regime. The third step is to low-pass filter and decimate the signal resulting from the second step to a lower sampling rate. The final step is to compute the squared enveloped signal followed by applying the Fourier transformation to obtain the Squared Enveloped Spectrum (SES).

As the resonance frequency of the low-cost sensor is around 75 Hz, the frequency band for applying the envelope analysis to the low-cost sensor signals was set to $[50, 90]$ Hz. On the other hand, the frequency band for applying the envelope analysis to the high-end sensor signals was selected by means of spectral kurtosis analysis using Kurtogram, as described in Antoni and Randall [13].

For a more rigorous comparison, the high-end sensor signals were also analysed with the Spectral Correlation (SC) technique to compute the "Enhanced Envelope Spectrum (EES)" being defined as:

$$S_x^{EES}(\alpha) = \int_{f_1}^{f_2} |\gamma_x(\alpha, f)| df \tag{3}$$

where $S_x^{EES}(\alpha)$ denotes the EES as a function of the cyclic frequency α that corresponds to the bearing fault frequency, f is the frequency, and $\gamma_x(\alpha, f)$ denotes the Spectral Coherence being defined as:

$$\gamma_x(\alpha, f) = \frac{S_x(\alpha, f)}{\sqrt{S_x(f) S_x(f - \alpha)}} \tag{4}$$

where $S_x(\alpha, f)$ denotes the SC being defined as the double discrete Fourier transform of the instantaneous autocorrelation function. The interested readers are referred to Antoni et al. [14] for detailed descriptions of the method.

4 Experiment

4.1 Characterisation of the low-cost sensor

Prior to using the low-cost sensor for bearing fault diagnosis, it was necessary to characterise the sensor and then compare the identified characteristics with the specifications provided by the supplier. To this end, an impact test was performed by hitting a structure on which the low-cost sensor was mounted. This impact test was repeated several times to check the repeatability. The impact response signal obtained from the low-cost sensor can be used for characterising the sensor by identifying the resonance frequency and damping factor.

4.2 Design of Experiment

One of the objectives of this study is to explore whether the low-cost sensor can be used to diagnose bearing faults under different loads and rotational speeds. In this study, a low speed is defined based on the criterion formulated in [11],

where the low-speed range is determined by the bearing pitch-line diameter. This criterion suggests that the low-speed range for the test bearing (N 203 ECP bearing) used in this study is below 100 rpm. Another consideration is the radial load range. According to the supplier mounting guideline, the minimum radial load that needs to be applied to the test bearing when it is in operation is 0.12 kN (12 kg). Based on these requirements, two radial loads (12.5 kg and 20 kg) and two rotational speeds (30 rpm and 60 rpm) were selected. Hence, there were four test conditions in total, namely (1) 12.5 kg and 30 rpm; (2) 12.5 kg and 60 rpm; (3) 20 kg and 30 rpm; and (4) 20 kg and 60 rpm. A fault with a dimension of 1 mm width and 1 mm depth was seeded on the outer race of the test bearing by means of the EDM wire-cutting technique as shown in Figure 6. The theoretical outer race fault frequency of this test bearing is about 3.7 Hz at 60 rpm shaft speed.

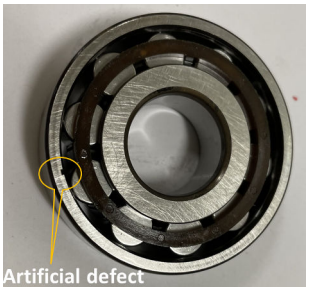

Figure 6: Test bearing with a seeded fault on the outer race.

Vibration signals from both the low-cost and high-end sensors were digitised and acquired using a PicoScope 4224 IEPE digital oscilloscope. All the signals were sampled at a sampling frequency of 20,000 Hz. The signal length for every data acquisition is 20 seconds to ensure that the shaft has rotated multiple revolutions.

5 Results and Discussions

5.1 Characteristics of the low-cost sensor

Figure 7 shows the signal of the low-cost sensor obtained from the impact test. Notably, the raw signal is mainly dominated by the electromagnetic interference (EMI) noise at the frequency of 50 Hz and some higher harmonics. After removing the EMI noise, the transient response is evident as seen in the figure. The Hankel Total Least Squares (HTLS) method, see Ompusunggu et al. [12], was applied to the filtered signal to identify the resonance frequency and the damping factor of the low-cost sensor. It was found that the estimated resonance frequency is around 75 Hz which is very close to the resonance frequency provided in the supplier datasheet. Figure 8 shows the frequency response of the low-cost sensor reconstructed by using the estimated resonance frequency and the damping factor.

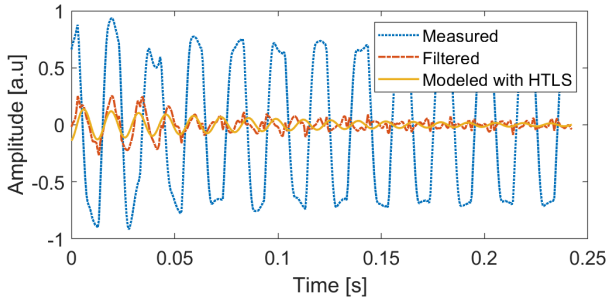

Figure 7: The impact response signal of the low-cost sensor.

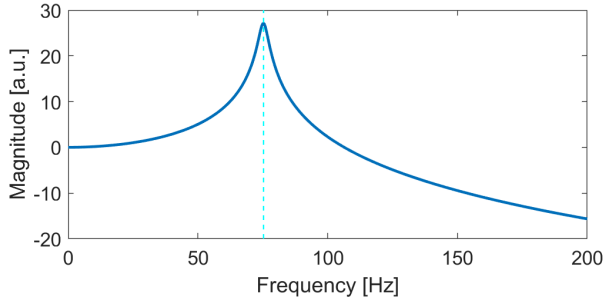

Figure 8: The estimated frequency response of the low-cost sensor. The vertical dashed line indicates the resonance frequency.

5.2 Signal analysis and fault diagnosis

Figure 9 show a representative time waveform of the low-cost sensor signal obtained from the most challenging case in this study, namely the lowest speed (i.e. 30 rpm) and the lowest radial load (i.e. 12.5 kg). As mentioned earlier, the raw signal of the low-cost sensor is highly contaminated by the EMI noise. However, after applying a comb filtering to the raw signal to remove the EMI noise and the higher harmonics, as theoretically predicted in Section 2, the low-cost sensor amplifies the repeated impulsive signature caused by the bearing fault in the vibration signal, as shown in the figure.

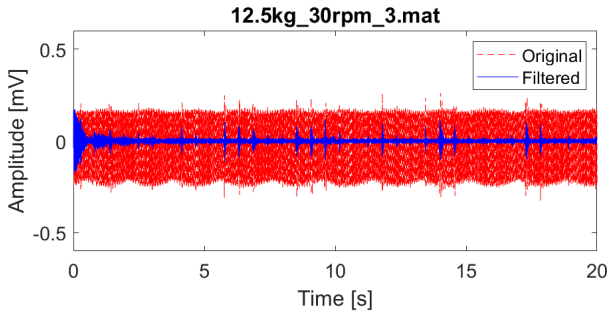

Figure 9: A representative time domain signal of the low-cost sensor. Note that the filtered signal (blue solid line) obtained after the removal of the EMI noise and the higher harmonics.

Figure 10 shows the frequency spectrum of the low-cost sensor signal obtained by applying the Fourier transformation to the signal shown in Figure 9. It is seen that the resonance frequency (see the peak around 75 Hz) of the low-cost sensor is clearly highlighted in the frequency spectrum. Notably, the EMI noise at 50 Hz and higher harmonics are evident as shown in the figure. Further examination of the frequency spectrum of the low-cost sensor signal, it is worth mentioning that there

also exist a few of resonance-induced phenomena around the frequencies of 25 Hz and 110 Hz that was captured by the sensor. However, at this stage it is not clear the origin of these resonance frequencies. Most likely that these resonance frequencies originate from the structure of the test rig, which will be investigated in the future. Notably, amplitude modulations around the resonance frequency of 25 Hz and 75 Hz can be observed in the frequency spectrum.

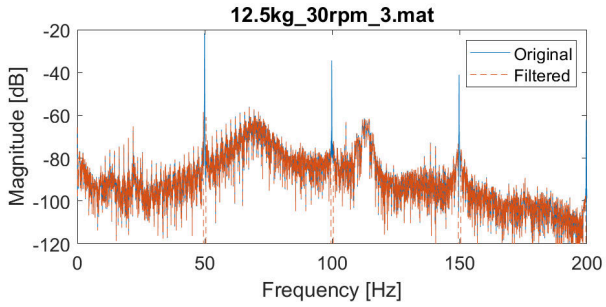

Figure 10: The frequency spectrum of the low-cost sensor signal in Figure 9.

For the high-end sensor signal, one can see in Figure 11 that no strong EMI noise was captured in the measurement. However, the high-end sensor signal does not show a clear repeated impulsive signature as opposed to the low-cost sensor signal (after the EMI noise removal).

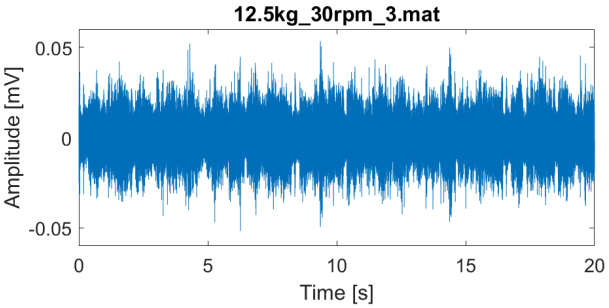

Figure 11: A representative time domain signal of the high-end sensor.

To further evaluate the high-end sensor signal, the frequency spectrum of the high-end sensor signal was calculated as shown in Figure 12. The frequency spectrum shows that the main signal components are concentrated at a high frequency range, around 240 and 490 Hz. For a fair comparison, the frequency spectrum of the high-end signal is zoomed in from 0 to 200 Hz, as shown if Figure 13. It is seen in the figure that amplitude modulations around the resonance frequency of 25 Hz and 75 Hz can also be observed in the frequency spectrum of the high-end signal. As both the high-end and low-cost sensors were mounted next to each other during the test, it is likely that the resonance of the low-cost sensor triggered by the impact excitation from the bearing fault was also captured by the high-end sensor.

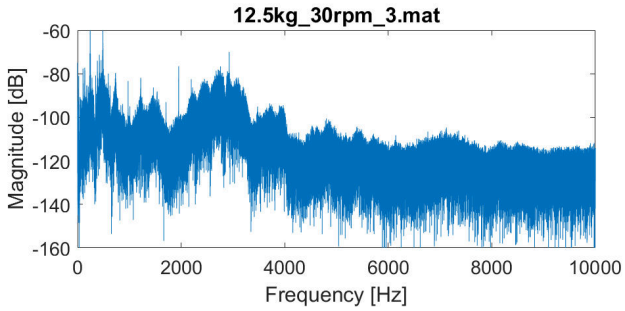

Figure 12: The frequency spectrum of the high-end sensor signal in Figure 11.

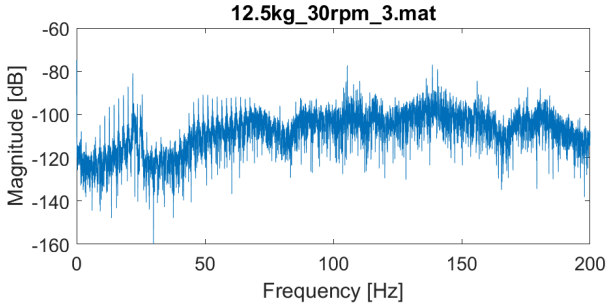

Figure 13: The zoomed-in frequency spectrum of the high-end sensor signal.

To verify this hypothesis, the the raw signal of the high-end sensor was analysed with the spectral kurtosis (SK) technique as mentioned in Section 3.3 From this SK analysis, the Kurtogram shown in Fig 14, from which a frequency band for performing the envelope analysis can be selected, is generated. For this test condition, the kurtogram suggests that the frequency band (with the central frequency of 65 Hz and the bandwidth of 30 Hz) for the envelope analysis should be selected. This frequency band is very close to the resonance frequency of the low-cost sensor, as mentioned earlier.

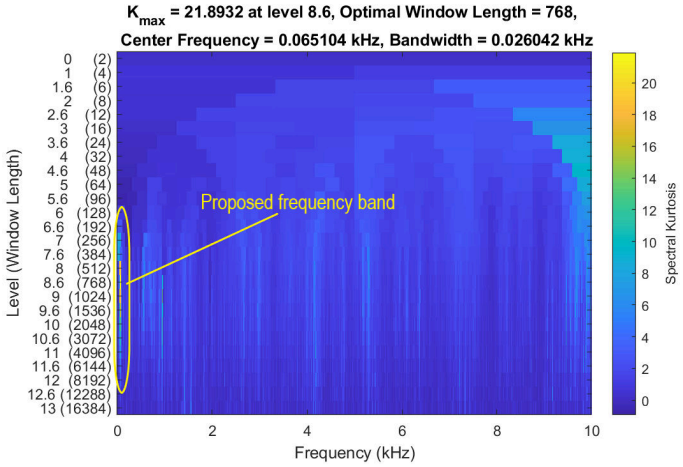

Figure 14: The Kurtogram obtained from the raw signal of the high-end sensor.

To decouple the resonance effect of the low-cost sensor, the high-end sensor raw signal was re-analysed with the SK technique. However, the raw signal was high-pass filtered with the cut-off frequency of 100 Hz prior to re-applying the SK technique. Figure 15 shows the kurtogram obtained after applying a high-pass filtering to the raw signal. For this test condition,

the kurtogram suggests that the frequency band with the central frequency of 0.95 kH and the bandwidth of 20 Hz, should be used for the envelope analysis.

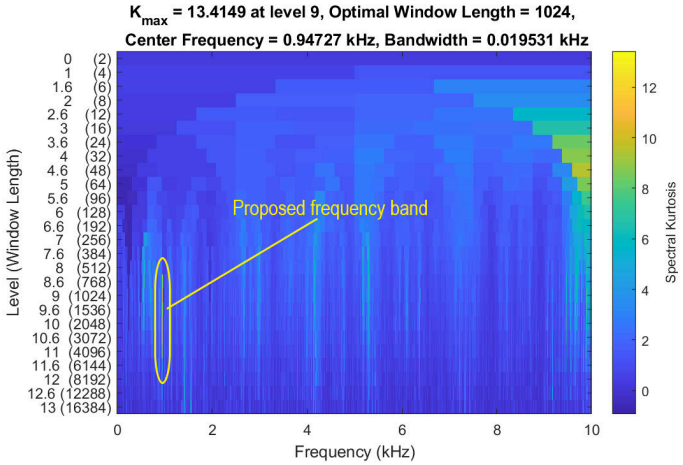

Figure 15: The Kurtogram obtained from the high-pass filtered signal of the high-end sensor with the cut-off frequency of 100 Hz.

For each test condition, the kurtogram was generated by applying the SK analysis technique to the high-pass filtered signal of the high-end sensor to determine the frequency band for the envelope analysis. The SES as mentioned in Section 3.3 were calculated from the high-end sensor signals. In addition to this, the EES were also calculated as a state-of-the art benchmark.

Figures 16 - 19 show the SES of the high-end and low-cost sensor signals and the EES of the high-end sensor signal, obtained from all the test conditions. The vertical dashed lines in the figures indicate the theoretical fault frequency and the higher harmonics. It is seen in the figures that the peaks in the SES match closely with the theoretical outer race fault frequency and the higher harmonics for the low-cost sensor, which suggests that the bearing fault was successfully diagnosed with the low-cost sensor and envelope analysis technique for the given test conditions.

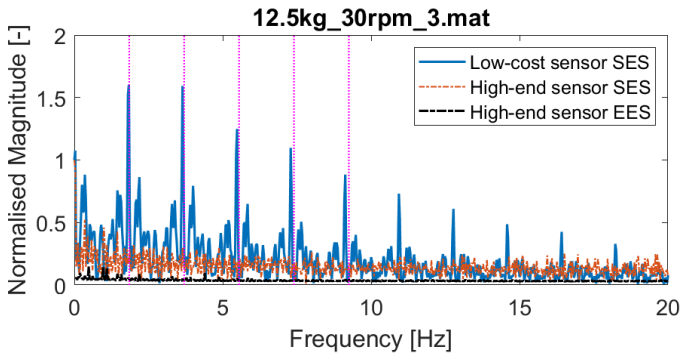

Figure 16: Envelope spectra of the outer race damaged bearing under 12.5 kg radial load and 30 rpm shaft speed obtained from the low-cost and high-end sensor signals.

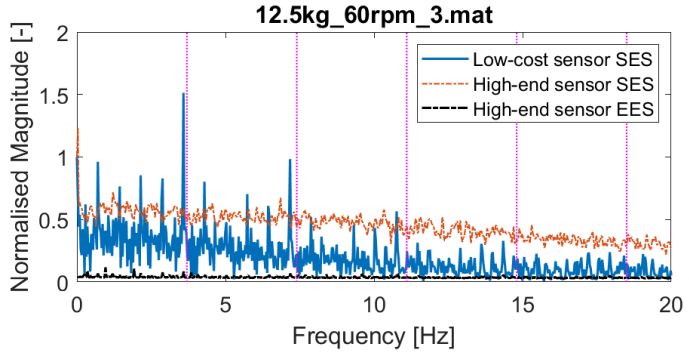

Figure 17: Envelope spectra of the outer race damaged bearing under 12.5 kg radial load and 60 rpm shaft speed obtained from the low-cost and high-end sensor signals.

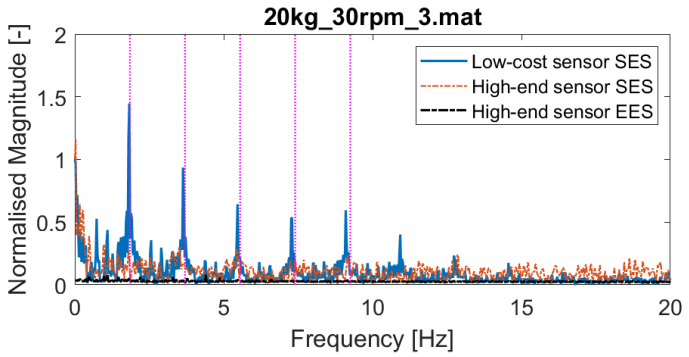

Figure 18: Envelope spectra of the outer race damaged bearing under 20 kg radial load and 30 rpm shaft speed obtained from the low-cost and high-end sensor signals.

On the other hand, the expected peaks around the theoretical fault frequency and the higher harmonics are not very obvious on the SES and EES of the high-end sensor for the following test conditions: (1) 12.5 kg radial load and 30 rpm, (2) 12.5 kg radial load and 60 rpm, and (3) 20 kg radial load and 30 rpm. This suggests that the high-end sensor signal analysed with the state-of-the art processing techniques was not able to detect and diagnose the bearing fault for such test conditions, see Figures 16 - 18.

However, as shown in Figure 19, the EES obtained by analysing the high-end sensor signal with the SC technique shows that the bearing outer race fault could still be detected for the test condition of 20 kg radial load and 60 rpm.

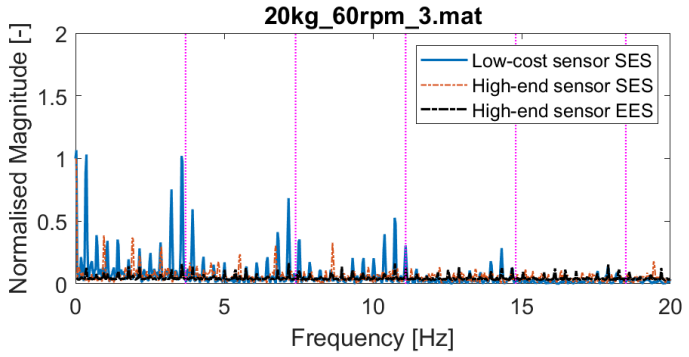

Figure 19: Envelope spectra of the outer race damaged bearing under 20 kg radial load and 60 rpm shaft speed obtained from the low-cost and high-end sensor signals.

6 Conclusion & Outlook

The feasibility to use a low-cost vibration sensor with low-resonance frequency for fault diagnosis of low-speed bearings has been demonstrated theoretically and experimentally in this paper. A low-cost vibration sensor with a resonance frequency of 75 Hz was selected from the market, tested on a low-speed bearing test rig recently developed at Cranfield University, and benchmarked with a high-end sensor (accelerometer). Four test conditions were selected in this feasibility study, namely (1) 12.5 kg radial load and 30 rpm, (2) 12.5 kg radial load and 60 rpm, (3) 20 kg radial load and 30 rpm, and (4) 20 kg radial load and 60 rpm. It was shown that the low-cost sensor analysed with the envelope analysis technique could successfully diagnose the outer race fault in a test bearing for all test conditions. On the other hand, the high-end sensor analysed with the state-of-the-art analysis technique (Spectral Correlation to compute an Enhanced Envelope Spectrum (EES)) could only detect and diagnose the bearing fault for the least challenging test condition, i.e. 20 kg radial load and 60 rpm. As the low-cost sensor signals were sampled at 400 Hz, a low-cost embedded platform with low computational power could be selected and integrated with the low-cost sensor for the development of a smart low-cost IoT vibration sensor.

It is worth mentioning that the low-cost sensor used in the study was not packaged. Hence, the measurement signals were significantly polluted by the electromagnetic interference (EMI) noise. In addition, a high-end charge amplifier available at Cranfield University was used with the low-cost sensor. Future work would be to develop a robust casing for the sensor to reduce the EMI noise and to package the sensor with an integrated charge amplifier.

7 Acknowledgments

The authors are grateful to the former MSc student, Zihao Yang, for designing/assembling the test rig and performing the test campaign as well as preliminary data analysis.

References

[1] Randall R.B.: "Vibration-based Condition Monitoring: Industrial, Aerospace and Automotive Applications", John Wiley, 2011.

[2] Kim E. Y., Tan A. C. C., Mathew J., and Yang B. S.: "Condition monitoring of low-speed bearings: A comparative study of the ultrasound technique versus vibration measurements", Australian Journal of Mechanical Engineering, 5:2, 177-189, 2008.

[3] Chen R., Tang L., Hu X., and Wu H.: "Fault Diagnosis Method of Low-Speed Rolling Bearing Based on Acoustic Emission Signal and Subspace Embedded Feature Distribution Alignment", *IEEE Transactions on Industrial Informatics*, vol. 17, no. 8, pp. 5402-5410, Aug. 2021.

[4] Ompusunggu A.P., Devos S., and Petre F.: "Stochastic-resonance based fault diagnosis for rolling element bearings subjected to low rotational speed", IJPHM, Vol. 4 No. 2, 2013.

[5] Shuuji M, Song X., Liao Z., and Chen P.: "Low-speed bearing fault diagnosis based on improved statistical filtering and convolutional neural network", 2021 Meas. Sci. Technol. 32 115009.

[6] Van Hecke B., Yoon J., and, He D.: "Low speed bearing fault diagnosis using acoustic emission sensors", Applied Acoustics, Vol. 105, Pages 35-44, 2016.

[7] Alshimmeri, F.: "Diagnosis of Low-Speed Bearing Degradation Using Acoustic Emission Techniques", PhD Thesis, Cranfield University, 2017.

[8] Hemmer, M.: "Condition Monitoring Methods for Large, Low-speed Bearings", PhD Thesis, University of Agder, 2020.

[9] Khanam, S., Dutt, J. K., and Tandon, N.: "Impact Force Based Model for Bearing Local Fault Identification", *ASME. J. Vib. Acoust.* October 2015; 137(5): 051002.

[10] Harris C. M., and Piersol A.G.: "Harris' Shock and Vibration Handbook", 5th Edition, McGraw-Hill, Book Company, 2002.

[11] https://www.kaydonbearings.com/downloads/whitepapers/Kaydon-LowSpeedAppsWP.pdf

[12] Ompusunggu A.P., Papy J.-M., Vandenplas S., Sas P., and Van Brussel H.: "A novel monitoring method of wet friction clutches based on the post-lockup torsional vibration signal", Journal of MSSP, Vol. 35, Issues 1–2, Pages 345-368, 2013.

[13] Antoni, J., and R. B. Randall.: "Fast Computation of the Kurtogram for the Detection of Transient Faults." Journal of MSSP. Vol. 20, Issue 1, 2007, pp. 108–124.

[14] Antoni J., Xin G., and Hamzaoui N.: "Fast computation of the spectral correlation", Journal of MSSP, Vol. 92, Pages 248-277, 2017.

Low-cost vibration sensor with low frequency resonance for condition monitoring of low speed bearings: a feasibility study

Ompusunggu, Agusmian Partogi

2023-09-27

Ompusunggu AP, Ruiz Carcel C. (2023) Low-cost vibration sensor with low frequency resonance for condition monitoring of low speed bearings: a feasibility study. In: 1st Workshop on Low-Cost Digital Solutions for Industrial Automation, 25-26 September 2023, Cambridge, UK
https://doi.org/10.1049/icp.2023.1748